Thermodynamics of Hg^{2+} and Ag^{+} adsorption by 3-mercaptopropionic acid functionalized superparamagnetic iron oxide nanoparticles

Sara Gràcia Lanas,[a,b] Manuel Valiente,[b] Marilena Tolazzi [a] and Andrea Melchior[a*]

[a]*DPIA, Laboratorio di Scienze e Tecnologie Chimiche, Università di Udine, Via del Cotonificio 108, 33100 Udine, Italy*

[b]*Departamento de Quimica, Centre GTS, Universitat Autònoma de Barcelona, Campus Bellaterra Edificio CN, Barcelona, Spain*

Abstract

Superparamagnetic iron nanoparticles (SPION) have been functionalized with 3-mercaptopropionic acid (3-MPA), characterized and applied for the removal of Ag^{+}, Hg^{2+} and Pb^{2+} metal ions from aqueous solutions by iron oxide (Fe_3O_4). The heavy metal adsorption has been investigated by means of ICP-OES and isothermal titration calorimetry. Experimental data ware better fitted by Langmuir rather than Freundlich isotherms and the thermodynamic parameters for the adsorption process of the metal ions on the functionalized SPION nanoparticles (SPION@3-MPA) were obtained.

Isothermal titration calorimetry (ITC) is applied to monitor heavy metal adsorption on SPION@3-MPA: the process results to be exothermic for Hg^{2+}, Ag^{+} while it is weakly endothermic in the case of Pb^{2+} and the adsorption enthalpies and entropies have been obtained. The values of the thermodynamic parameters suggest that the Ag^{+} and Hg^{2+} ions interact strongly with the thiol groups, while the Pb^{2+} ions seem to be adsorbed by the material mostly *via* electrostatic interaction. When compared to other thiol-functionalized materials, the obtained SPION@3-MPA NP can be considered a competitive adsorbent for Ag^{+} and Hg^{2+} ions. The comparison between the ICP-OES adsorption rata and the enthalpy trend obtained by ITC supports shows that the latter technique can be a good tool for a fast testing of materials to be applied for heavy metal separation from solutions.

*Corresponding author's email: andrea.melchior@uniud.it
phone: +39 0432 558882

Keywords: superparamagnetic iron oxide nanoparticles; surface functionalization; isothermal titration calorimetry; mercury; silver; adsorption

1. Introduction

Activities such as electroplating, mining, metallurgical and chemical industries are some of the main anthropogenic sources of heavy metals (HM) in the environment[1]. Unlike organic contaminants, heavy metals are not biodegradable, tend to accumulate in living organisms[2] and soils[3,4]. Heavy metals also can enter the food chain[5] and are known to be toxic or carcinogenic[4,6,7]. Due to such serious consequences, the release of heavy metal contaminants in the environment has to be avoided and therefore it is of fundamental importance to have efficient methods for the HM recovery from liquid wastes. Several methods of heavy metal ion removal have been developed so far[8], but they suffer from several issues, such as complicated processes, high costs, secondary pollution and recycling difficulty. In contrast, adsorption, is one of the best techniques recognized as effective wastewater treatment because it offers flexibility in design and operation and sustainability both from an environmental and economic point of view[9]. Furthermore, since this process is often reversible, adsorbed species can be recovered by suitable desorption process and the material regenerated for its re-use.

Nanoparticles attracted much attention for metal ion recovery from water because of their high surface area to volume ratio, fast reaction kinetics, the possibility to be chemically modified on their surface[10,11]. These materials can be then separated from the liquid samples with relatively simple methods. Among them, nanosized metal oxides demonstrated to be promising materials for metal removal from wastewaters[9,12,13]. Recently, Super Paramagnetic Iron Oxide Nanoparticles (SPION), received special attention for their low toxicity, low cost and easy recovery from aqueous media by magnetic separation[9,14,15]. To obtain an efficient recovery of metal ions from aqueous solutions it is necessary to modify the surface of the SPION with organic ligands able to bind selectively a given metal ion.

In this work, SPION functionalized with 3-mercaptopropionic acid (SPION@3-MPA) are synthesized characterized and tested for the removal of heavy metal ions from water. This nanomaterial has been previously employed for the adsorption of anionic inorganic pollutants[16–19], but never for heavy metal cation removal from water, despite the

presence of thiol groups makes it particularly suitable for the selective separation of heavy metal cations with a soft acid nature. The adsorption of Ag^{+}, Hg^{2+} and Pb^{2+} is studied by means of a combination of ICP-OES analysis and Isothermal Titration Calorimetry (ITC). Calorimetry is a powerful tool which allows to directly measure the energy exchange occurring when two reagents are mixed in the measurement cell. This technique has been largely used to obtain thermodynamic data for metal complexation reactions occurring in aqueous or non-aqueous media[20–29], but much less examples of ITC applied to metal ion adsorption studies are present in the literature[30–37]. In many works, metal ion adsorption enthalpy (ΔH_{ads}) has been calculated by van't Hoff equation[38,39]. However, the values obtained by this method often suffer from relatively large uncertainties[40]. Moreover, several studies evidenced serious discrepancies with enthalpies obtained by direct calorimetric measurements[41–46]. In this work, ITC is applied for the direct determination of ΔH_{ads} to provide reliable thermodynamic parameters for metal ion adsorption.

2. Materials and methods

2.1. *Chemicals*

All reagents used in the experiment were analytical grade and used without further purification. Ammonium hydroxide (NH_4OH), hydrochloric acid (HCl), Fe(II) chloride ($FeCl_2 \cdot 4H_2O$), Fe(III) chloride ($FeCl_3 \cdot 6H_2O$) and 3-mercaptopropionic acid (3-MPA) were purchased from Sigma-Aldrich.

The metal stock solutions were prepared by dissolving Hg(II) chloride ($HgCl_2$, Riedel), lead(II) nitrate ($Pb(NO_3)_2$ Fluka), silver perchlorate ($AgClO_4$, Aldrich) in acetic acid / acetate buffer.

2.2. Synthesis and functionalization of SPION

Iron oxide nanoparticles were synthesized by a co-precipitation method, similar to that described elsewhere[17]. The formation of the particles is schematized in Eq.1:

$$FeCl_2 + 2FeCl_3 + 8NH_4OH \rightarrow Fe_3O_4(colloid) + 8NH_4Cl + 4H_2O \quad (1)$$

A stock solution of NH_4OH 0.7M was deoxygenated under nitrogen gas with vigorous magnetically stirring and heated at 70 °C. The stock solution of Fe(III) and Fe(II) was prepared dissolving the respective chloride salts (Fe(II) : Fe(III) in a molar ratio 1 : 2) in a deoxygenated HCl 0.2M and then added to the NH_4OH solution. The particles obtained (solution turned black quickly) were aged during 45 min and then cooled to room temperature with a water bath. The SPION were collected by a magnetic separation and then washed several times with deoxygenated distilled water. The synthesis was carried out in a continuous N_2 bubbling, in order to avoid the oxidation of Fe(II) into Fe(III) and the formation of undesirable iron oxides as maghemite or ferrihydrite.

The SPION@3-MPA were obtained by ligand addition method[17]. A known amount of SPION was suspended in water acidified with HNO_3 to pH = 2.0, to have the surface charged positively (pH_{pzc} of the SPION = 6.8)[47]. Then, 10 mL of suspension was added a solution of the 3-MPA (150 mM) in toluene and stirred continuously for 24h under N_2 atmosphere.

2.3. Material characterization

The nanoparticles were imaged by Scanning Electron Microscope (SEM) using a MERLIN FE-SEM (Carl Zeiss Microscopy, LLC., Germany) with an EDS detector Oxford LINCA X-Max and EBSD analysis Oxford Nordlys II. Transmission Electron Microscope (TEM) micrographs were performed by JEM-2011, with a resolution of 0.18 nm at 200 kV and an accelerating voltage of 80–200kV and equipped with a camera CCD GATAN 895 USC 4000 and a detector EDS Oxford LINCA with energy resolution of 136eV (Jeol Ltd., Japan).

The crystallographic phase determination was obtained by X-ray diffraction (XRD) of the powder with a Philips X-Pert diffractometer using a nickel-filtered Cu K_α radiation. The diffractograms were collected in the 2θ range of 15–100° with a step of 0.02 and a counting time of 15 s/step.

The BET surface area data were calculated from N_2 adsorption at -196 °C by using a Micromeritics Tristar 3000 gas adsorption analyzer. Prior to the analysis, the samples were kept at 150°C for 1h under vacuum conditions.

Particle size distribution was determined by dynamic light scattering (DLS) on a Horiba LB-550 Particle Size Analyzer. A sample of SPION was suspended in 10 mL of water and sonicated for 15 min before the DLS measurement.

Vibrational spectra were recorded before and after functionalization with 3-MPA in the middle-IR region (400 - 4000cm^{-1}) using a VECTOR 22 FT-IR spectrometer equipped with a ATR accessory.

Thermogravimetric (TGA) analysis was performed with a Q500 TGA (TA Instruments) to determine the amount of 3-MPA present on the SPION. A sample (15-20 mg) was placed in a small flat Pt crucible licked by a tangent N_2 flow (60ml min^{-1}) and then heated at a constant rate (10 °C min^{-1}) up to 900°C. The pH_{pzc} of SPION@3-MPA was determined by the published methodology[48].

2.4. Adsorption studies

The adsorption experiments were performed at room temperature (298K ±1) in batch conditions by adding 5mg of SPION@3-MPA to 10mL solutions containing metal ions in the 0.1-1.0 mM concentration range. The suspension was sonicated during 30min and then allowed 30min in contact. The magnetic adsorbent was separated from the aqueous phase and the metal concentration in the filtered solution was determined by ICP-OES (Varian VISTA-MPX CCD Simultaneous ICP-OES).

Adsorption of Pb^{2+}, Hg^{2+} and Ag^{+} was carried out at pH = 5.0 (20mM acetic acid buffer solution). At higher pH (> 5.0) these metals can hydrolyse and the corresponding hydroxide precipitates ($M(OH)_n$). On the other hand, at pH extremely acidic, the surface of the adsorbent material would be highly protonated inhibiting the adsorption due to electrostatic repulsions.

Adsorption data were fitted by Freundlich and Langmuir isotherms, since it has been demonstrated that such models better fit the adsorption behaviour of pollutants from solutions[49]. The aforementioned models may be expressed by Eq. 2 and Eq. 3 respectively[50–52]:

$$C_{ads} = \frac{Q_{\max} b C_e}{1 + b C_e} \qquad (2)$$

C_e = equilibrium concentration (M), C_{ads} = solute adsorbed at equilibrium (mol g^{-1}), $Q_{\max}$ = maximum quantity of solute adsorbed per gram of adsorbent (mol g^{-1}) and b = Langmuir constant (M^{-1}).

$$C_{ads} = K_f C_e^{\frac{1}{n}} \qquad (3)$$

K_f = Freundlich constant ($(L \cdot mmol^{-1}\ g^{-1})^{1/n}$), n = adsorption intensity, C_e = equilibrium concentration of the metal ion in the solution (M), C_{ads} = amount of adsorbed species at equilibrium (mol g^{-1}).

2.5. Isothermal Titration Calorimetry (ITC)

The calorimetric study of adsorption was carried out with a TAMIII isothermal microcalorimeter (TA Instruments) connected with an automatic titration syringe was used to measure the heat of adsorption of the metals on SPION@3-MPA. The samples were prepared in acetic-acetate buffer solutions (pH = 5.0). The titration cell was filled with 0.7mL of buffer where ~0.5g L^{-1} SPION@3-MPA were dispersed. The suspension was stirred continuously at 120rpm. The cell content was titrated with 14μL injections of $Ag^{+}$and Hg^{2+} solutions (metal concentrations ~5mM) and 12 injections of 16μL of Pb^{2+} (4.2mM). A delay time of 1 hour between consecutive injections was set for all metals. The reference cell was filled with 0.8 mL of MilliQ water.

The values of b and Q_{max} resulted from the fit of the Langmuir isotherm obtained from ICP-OES data have been used as input data in eq. 4 to calculate C_e for each titrant addition by numerically solving eq. 2 with the same experimental conditions as the calorimetric titrations[53]. Then, the ΔH_{ads} (kJ mol^{-1}) value has been calculated to best fit the experimental heat according to the isotherm (eq. 4):

$$q_{cum} = \frac{Q_{max} b C_e}{1 + b C_e} \Delta H_{ads} \qquad (4)$$

Where: q_{cum} = total heat involved at each titrant addition per weight (w) of adsorbent (kJ g^{-1}). Dilution heat (q_{dil}) was also determined to correct the total heat measured (q_{meas}) by the instrument. Thus $q_{cum} = (q_{meas} - q_{dil})/w$ represents only the heat involved on the adsorption reaction. Data fitting and statistical analysis of the results has been done with the MS-Excel Solverstat and EST tools[54,55].

3. Results and Discussion

3.1. Material characterization

The BET surface area for bare SPION has been found to be 92.3 m^2 g^{-1}, while resulted in 63.4m^2 g^{-1} for SPION@3-MPA. Therefore, the surface area decreases when the particles are coated by the organic ligand.

The SPION@3-MPA diffractogram (Figure S1, Electronic Supplementary Material) exhibits a single phase analogous to the characteristic reflections of magnetite (Fe_3O_4), corresponding to the (111), (220), (311), (400), (422), (511) and (400) planes as confirmed by JCPDS database (JCPDS, Card N°19). This shows that the 3-MPA coating process does not cause modifications of the crystalline phase of the material.

The vibrational spectrum of SPION (Figure 1) shows a band at 524 cm^{-1}, characteristic of Fe-O vibrations [12]. The spectrum of the free 3-MPA ligand displays a peak at 3100 cm^{-1}, which corresponds to the O-H vibrations, while the presence of the functional group S-H is evidenced by the two weak bands at 2669 cm^{-1} and 2573 cm^{-1}. The strong band at 1710 cm^{-1} identifies the C=O vibrations, and the two peaks at 1433 cm^{-1} and 1251 cm^{-1} are assigned to the C-O- stretching.

The SPION@3-MPA would be expected to present a stretching band around 2573 cm^{-1}, related to S-H stretching, however, because of its weak intensity it is typically not observed in thin films [12]. Two new bands corresponding to the symmetric and asymmetric stretching modes of a bidentate bound carboxylate group[56] appear at 1540 cm^{-1} and 1400 cm^{-1}. All these features in the vibrational spectra clearly indicate that the binding of the ligand to the SPION surface occurs through the carboxylate group rather than the thiol one as shown in Figure 2, as previously suggested[12,17].

Thermogravimetric analysis (Figure 3) displays an initial weight loss about 1% for both SPION and SPION@3-MPA is observed until 200°C, which is related to the loss of internal hydroxyl groups and/or adsorbed water[57]. The 0.8% of weight loss for bare SPION above 200°C is related to the decomposition of amorphous iron hydroxides followed by iron oxide formation[16], while the 12.9% of mass loss of the coated SPION is associated to the decomposition of the 3-MPA attached on the particles surface[16]. Thus, TGA analysis confirm the functionalization of the NP with an amount of 1.4 mmol g^{-1} of 3-MPA coating the SPION surface.

The SEM and TEM images of SPION@3-MPA are shown in Figure 4. In the SEM images (Figure 4-A and B), the particles appear spherical with some aggregation, possibly related to the coating of the NP. TEM micrographs (Figure 4-C and D), show that the particles have a mean diameter of 10-30nm. Aggregation is also confirmed by DLS (Figure S2), which provides an average size of ~890 nm.

3.2. Metal ions adsorption

The pH_{pzc} obtained for SPION@3-MPA is pH_{pzc} = 4.0. Hence, pH_{pzc} of the coated SPION shifted from 6.8[47] for uncoated SPION to 4.0 for the functionalized material. Therefore, when the working pH is higher than pH_{pzc} (4.0), the SPION@3-MPA surface is negatively charged while it will be positively charged at lower pH. This implies that the metal ions studied will be attracted by electrostatic force towards the surface in the conditions employed for the adsorption study.

The adsorption data have been fitted with Langmuir and Freundlich isotherms and the obtained parameters are summarized in Table 1, while the experimental points and calculated curves are reported in Figure 5. The best fit is always obtained when the Langmuir model is used (Table 1), indicating the presence of a monolayer adsorption. The Langmuir adsorption constant (*b*) obtained for each metal ion is considerably high, with log*b* values similar for Hg^{2+} and Ag^{+}, higher than that for Pb^{2+} ion. The Q_{max} shows a similar loading capacity for Hg^{2+} and Ag^{+}, which is ~11 times higher than that obtained for Pb^{2+} ion. When Q_{max} is compared with the number of moles of 3-MPA bound to SPION, it emerges that a ~1:1 metal/ligand ratio is obtained in the case of Hg^{2+} and Ag^{+}.

The calorimetric titrations of SPION@3-MPA suspensions with solutions of the ions are shown in Figure 6, and the experimental and calculated q_{cum} values are reported in Figure 7, as obtained by using eq. 4. The corresponding ΔH_{ads} are reported in Table 2 together with the calculated entropy values.

The ΔH_{ads} is clearly negative for Ag^{+} and Hg^{2+}, while for Pb^{2+} a weak endothermic effect is shown. The calorimetric data are therefore in agreement with a weaker interaction of $Pb^{2+}$with the SPION@3-MPA particles. Also, adsorption takes place with a positive entropy change (ΔS_{ads}) for Ag^{+}, Hg^{2+} and Pb^{2+}, indicating an increase of the degrees of freedom of the system which is related to the desolvation of the metal ions when interacting with the SPION@3-MPA surface and with the solution reorganization upon charge neutralization[58–60]. The obtained ΔS_{ads} for the Ag^{+} adsorption process is

relatively small with respect to the bipositive ions in agreement with its lower solvation in water[58–60].

The enthalpy values indicate that Ag^+ and Hg^{2+}interact more strongly with the thiol groups of 3-MPA bound to SPION surface with respect to Pb^{2+}, in agreement with their soft acid nature[21,61,62]. The Pb^{2+} ions seem to interact mostly *via* electrostatic interaction with the negatively charged surface[63] as suggested by the small positive ΔH_{ads} and large ΔS_{ads}. Furthermore, the possible species formed should be taken into account in an adsorption experiment, since they can strongly influence the process (and the thermodynamic parameters associated). On the basis of available stability constants data[64–66], in our experimental conditions, the Ag^+ is essentially present as hydrated ion, while Pb^{2+} and Hg^{2+} are partially complexed by the acetate of the buffer. In this respect, further studies in different ionic media and/or complexing species that could modulate the selectivity of the SPION@3-MPA nanoparticles will follow.

The simultaneous fitting the ΔH_{ads}, b and Q_{max} parameters does not lead to meaningful results since they are affected by very large error. However, if the Q_{max} is determined independently (or estimated) and only ΔH_{ads}, b are optimized, the results obtained are not far from those obtained by the combined ITC-ICP method (Table S1).

Adsorption data for SPION@3-MPA with the metals reported in this work and for some thiol-functionalized adsorbents found in the literature are reported in Table 3[67–73].

The SPION@3-MPA nanoparticles show better loading capacity for Ag^+ (1.5mmol g^{-1}) than the silica NP modified with trithiocyanuric acid[67] (0.75 mmol g^{-1}) or thiol-functionalized silica[68] (0.70mmol g^{-1}), while exhibit a lower adsorption capacity regarding the thiol-functionalized polysilsesquioxane microspheres (10.57 mmol g^{-1})[69]. The Q_{max} obtained for Hg^{2+} adsorption (1.7mmol g^{-1}) is higher than for other materials reported in the literature, when comparing SPION@3-MPA with Fe_3O_4@SiO_2–SH[70] (0.74mmol g^{-1}) or respect to thiol-functionalized superparamagnetic carbon nanotubes[71] (0.33mmol g^{-1}), however a lower adsorption capacity is observed when compared with $CoFe_2O_4$@SiO_2–SH (3.19mmol g^{-1}) [72].

The adsorption efficiency of the SPION@3-MPA towards Pb^{2+} (0.14mmol g^{-1}) is poorer when compared with other materials (Table 3)[67,71–73].

4. Conclusions

The SPION@3-MPA nanoparticles are a low-cost material which can be dispersed in the solution containing the target species and then easily recovered by the application of a magnetic field.

The adsorption of Ag^+, Hg^{2+} and Pb^{2+} ions by the SPION@3-MPA is well modelled by a Langmuir isotherm. The log*b* values are similar for Hg^{2+} and Ag^+ while somewhat lower for Pb^{2+}. On the contrary, the loading capacity, which is much higher for Hg^{2+} and Ag^+ ions makes SPION@3-MPA nanoparticles suitable for their recovery.

Calorimetric data show that adsorption on SPION@3-MPA is an exothermic process for Hg^{2+}, Ag^+ while it is weakly endothermic in the case of Pb^{2+}. The enthalpy trend obtained by ITC parallels the affinity sequence found by ICP-OES, evidencing that also calorimetry is a good tool for screening adsorbent materials.

The adsorption enthalpy values, negative for Ag^+ and Hg^{2+} and positive for Pb^{2+}, suggest that the ions interact differently with the SPION@3-MPA. In particular Ag^+ and Hg^{2+} show stronger interactions with the thiol groups, while the Pb^{2+} ions seem to interact mostly *via* electrostatic interaction with the negatively charged surface. This is compatible also with the ΔS_{ads} values, much more positive for Pb^{2+} than the other two ions.

When compared to some other thiol-functionalized materials, the obtained SPION@3-MPA NP can be considered an interesting adsorbent for Ag^+, Hg^{2+} ions, while a lower efficacy is found towards the Pb^{2+} ion.

Acknowledgments

The authors would like to thank Dr. Eleonora Aneggi for the assistance with material characterization.

Bibliography

1. Chowdhury S, Mazumder MAJ, Al-Attas O, Husain T. Heavy metals in drinking water: Occurrences, implications, and future needs in developing countries. Sci. Total Environ. 2016;569–570:476–88.

2. Khan A, Khan S, Khan MA, Qamar Z, Waqas M. The uptake and bioaccumulation of heavy metals by food plants, their effects on plants nutrients, and associated health risk: a review. Environ. Sci. Pollut. Res. 2015;22:13772–99.

3. Sherameti I, Varma A, editors. Heavy Metal Contamination of Soils. Springer International Publishing; 2015.

4. Kim K-H, Kabir E, Jahan SA. A review on the distribution of Hg in the environment and its human health impacts. J. Hazard. Mater. 2016;306:376–85.

5. Bosch AC, O'Neill B, Sigge GO, Kerwath SE, Hoffman LC. Heavy metals in marine fish meat and consumer health: A review. J. Sci. Food Agric. 2016;96:32–48.

6. Papanikolaou NC, Hatzidaki EG, Belivanis S, Tzanakakis GN, Tsatsakis AM. Lead toxicity update. A brief review. Med. Sci. Monit. 2005;11:RA329-336.

7. Ratte HT. Annual Review Bioaccumulation and toxicity of silver compounds: A Review. Environ. Toxicol. Chem. 1999;18:89–108.

8. Fu F, Wang Q. Removal of heavy metal ions from wastewaters: A review. J. Environ. Manage. 2011;92:407–18.

9. Hua M, Zhang S, Pan B, Zhang W, Lv L, Zhang Q. Heavy metal removal from water/wastewater by nanosized metal oxides: A review. J. Hazard. Mater. 2012;211–212:317–31.

10. Khajeh M, Laurent S, Dastafkan K. Nanoadsorbents: Classification, preparation, and applications (with emphasis on aqueous media). Chem. Rev. 2013;113:7728–68.

11. Kefeni KK, Mamba BB, Msagati TAM. Application of spinel ferrite nanoparticles in water and wastewater treatment: A review. Sep. Purif. Technol. 2017;188:399–422.

12. Warner CL, Addleman RS, Cinson AD, Droubay TC, Engelhard MH, Nash MA, Yantasee W, Warner MG. High-performance, superparamagnetic, nanoparticle-based heavy metal sorbents for removal of contaminants from natural waters. ChemSusChem. 2010;3:749–57.

13. Yantasee W, Warner CL, Sangvanich T, Addleman RS, Carter TG, Wiacek RJ, Fryxell GE, Timchalk C, Warner MG. Removal of heavy metals from aqueous systems with thiol functionalized superparamagnetic nanoparticles. Environ. Sci. Technol. 2007;41:5114–9.

14. Singh N, Jenkins GJS, Asadi R, Doak SH. Potential toxicity of superparamagnetic iron oxide nanoparticles (SPION). Nano Rev. 2010;1:5358.
15. Mariani G, Fabbri M, Negrini F, Ribani PL. High-Gradient Magnetic Separation of pollutant from wastewaters using permanent magnets. Sep. Purif. Technol. 2010;72:147–55.
16. Burks T, Avila M, Akhtar F, Göthelid M, Lansåker PC, Toprak MS, Muhammed M, Uheida A. Studies on the adsorption of chromium(VI) onto 3-Mercaptopropionic acid coated superparamagnetic iron oxide nanoparticles. J. Colloid Interface Sci. 2014;425:36–43.
17. Morillo D, Uheida A, Pérez G, Muhammed M, Valiente M. Arsenate removal with 3-mercaptopropanoic acid-coated superparamagnetic iron oxide nanoparticles. J. Colloid Interface Sci. 2015;438:227–34.
18. Kim C, Lee SS, Lafferty BJ, Giammar DE, Fortner JD. Engineered superparamagnetic nanomaterials for arsenic(V) and chromium(VI) sorption and separation: quantifying the role of organic surface coatings. Environ. Sci. Nano. 2018;5:556–63.
19. Melchior A, Lanas SG, Valiente M, Tolazzi M. Thermodynamics of sorption of platinum on superparamagnetic nanoparticles functionalized with mercapto groups. J. Therm. Anal. Calorim. 2018; DOI: 10.1007/s10973-018-7408-3
20. Cavallo L, Del Piero S, Ducéré J, Fedele R, Melchior A, Morini G, Piemontesi F, Tolazzi M. Key Interactions in Heterogeneous Ziegler - Natta Catalytic Systems : Structure and Energetics of $TiCl_4$-Lewis Base Complexes. J. Phys. Chem. C. 2007;111:4412–9.
21. Melchior A, Peralta E, Valiente M, Tavagnacco C, Endrizzi F, Tolazzi M. Interaction of d(10) metal ions with thioether ligands: a thermodynamic and theoretical study. Dalton Trans. 2013;42:6074–82.
22. Bernardo P Di, Zanonato PL, Melchior A, Portanova R, Tolazzi M, Choppin GR, Wang Z. Thermodynamic and Spectroscopic Studies of Lanthanides (III) Complexation with Polyamines in Dimethyl Sulfoxide. Inorg. Chem. 2008;47:1155–64.
23. Melchior A, Gaillard C, Gràcia Lanas S, Tolazzi M, Billard I, Georg S, Sarrasin L, Boltoeva M. Nickel(II) Complexation with Nitrate in Dry $[C_4\,mim][Tf_2N]$ Ionic Liquid: A Spectroscopic, Microcalorimetric, and Molecular Dynamics Study. Inorg. Chem. 2016;55:3498–507.
24. Endrizzi F, Di Bernardo P, Zanonato PL, Tisato F, Porchia M, Ahmed Isse A, Melchior A, Tolazzi M. Cu(I) and Ag(I) complex formation with the hydrophilic

phosphine 1,3,5-triaza-7-phosphadamantane in different ionic media. How to estimate the effect of a complexing medium. Dalt. Trans. 2017;46:1455–66.
25. Endrizzi F, Melchior A, Tolazzi M, Rao L. Complexation of uranium(VI) with glutarimidoxioxime: thermodynamic and computational studies. Dalt. Trans. 2015;44:13835–44.
26. Del Piero S, Di Bernardo P, Fedele R, Melchior A, Polese P, Tolazzi M. Affinity of Polypyridines Towards Cd(II) and Co(II) Ions: a Thermodynamic and DFT Study. Eur. J. Inorg. Chem. 2006;2006:3738–45.
27. Credendino R, Minenkov Y, Liguori D, Piemontesi F, Melchior A, Morini G, Tolazzi M, Cavallo L. Accurate experimental and theoretical enthalpies of association of TiCl 4 with typical Lewis bases used in heterogeneous Ziegler–Natta catalysis. Phys. Chem. Chem. Phys. 2017;19:26996–7006.
28. Melchior A, Peressini S, Portanova R, Sangregorio C, Tavagnacco C, Tolazzi M. Cobalt(II) and cadmium(II) chelates with nitrogen donors and O2 bonding to Co(II) derivatives. Inorg. Chim. Acta. 2004;357:3473–82.
29. Del Piero S, Melchior A, Polese P, Portanova R, Tolazzi M. N-Methylation Effects on the Coordination Chemistry of Cyclic Triamines with Divalent Transition Metals and Their Co(II) Dioxygen Carriers. Eur. J. Inorg. Chem. 2006;2006:304–14.
30. Braga PRS, Costa AA, de Macedo JL, Ghesti GF, de Souza MP, Dias JA, Dias SCL. Liquid phase calorimetric-adsorption analysis of Si-MCM-41: Evidence of strong hydrogen-bonding sites. Microporous Mesoporous Mater. 2011;139:74–80.
31. Arakaki LNH, Filha VLSA, Germano AFS, Santos SSG, Fonseca MG, Sousa KS, Espínola JGP, Arakaki T. Silica gel modified with ethylenediamine and succinic acid-adsorption and calorimetry of cations in aqueous solution. Thermochim. Acta. 2013;556:34–40.
32. Silva Filho EC, Lima LCB, Sousa KS, Fonseca MG, Pereira FAR. Calorimetry studies for interaction in solid/liquid interface between the modified cellulose and divalent cation. J. Therm. Anal. Calorim. 2013;114:57–66.
33. F. S.Vieira Eunice, de A. Simoni J, Airoldi C. Interaction of cations with SH-modified silica gel: thermochemical study through calorimetric titration and direct extent of reaction determination. J. Mater. Chem. 1997;7:2249–52.
34. Fonseca M da. Phyllosilicate-like structure anchored silylating agents: calorimetric data on divalent cation- aminated centre interactions in the lamellar cavity. J. Chem. Soc., Dalt. Trans. 1999;259:3687–92.

35. Evangelista SM, DeOliveira E, Castro GR, Zara LF, Prado AGS. Hexagonal mesoporous silica modified with 2-mercaptothiazoline for removing mercury from water solution. Surf. Sci. 2007;601:2194–202.
36. Zhang N, Zang GL, Shi C, Yu HQ, Sheng GP. A novel adsorbent TEMPO-mediated oxidized cellulose nanofibrils modified with PEI: Preparation, characterization, and application for Cu(II) removal. J. Hazard. Mater. 2016;316:11–8.
37. Huang Y, Keller AA. Isothermal titration microcalorimetry to determine the thermodynamics of metal ion removal by magnetic nanoparticle sorbents. Environ. Sci. Nano. 2016;3:1206–14.
38. Elwakeel KZ, El-Sayed GO, Darweesh RS. Fast and selective removal of silver(I) from aqueous media by modified chitosan resins. Int. J. Miner. Process. 2013;120:26–34.
39. Liang X, Xu Y, Sun G, Wang L, Sun Y, Sun Y, Qin X. Preparation and characterization of mercapto functionalized sepiolite and their application for sorption of lead and cadmium. Chem. Eng. J. 2011;174:436–44.
40. Gràcia Lanas S, Valiente M, Aneggi E, Trovarelli A, Tolazzi M, Melchior A. Efficient fluoride adsorption by mesoporous hierarchical alumina microspheres. RSC Adv. 2016;6:42288–96.
41. Liu Y, Sturtevant JM. Significant discrepancies between van't Hoff and calorimetric enthalpies. II. Protein Sci. Cold Spring Harbor Laboratory Press; 1995;4:2559–61.
42. Chaires JB. Possible origin of differences between van't Hoff and calorimetric enthalpy estimates. Biophys. Chem. 1997;64:15–23.
43. Liu Y, Sturtevant JM. Significant discrepancies between van't Hoff and calorimetric enthalpies. III. Biophys. Chem. 1997;64:121–6.
44. Mizoue LS, Tellinghuisen J. Calorimetric vs. van't Hoff binding enthalpies from isothermal titration calorimetry: Ba^{2+}-crown ether complexation. Biophys. Chem. 2004;110:15–24.
45. Welsch N, Lu Y, Dzubiella J, Ballauff M. Adsorption of proteins to functional polymeric nanoparticles. Polymer (Guildf). 2013;54:2835–49.
46. Teodoro FS, Ramos SN do C, Elias MMC, Mageste AB, Ferreira GMD, da Silva LHM, Gil LF, Gurgel LVA, Adarme OFH, Gil LF, Gurgel LVA. Synthesis and application of a new carboxylated cellulose derivative. Part II: Removal of Co^{2+}, Cu^{2+} and Ni^{2+} from bicomponent spiked aqueous solution. J. Colloid Interface Sci. 2017;487:266–80.
47. Yean S, Cong L, Yavuz CT, Mayo JT, Yu WW, Kan AT, Colvin VL, Tomson MB.

Effect of magnetite particle size on adsorption and desorption of arsenite and arsenate. J. Mater. Res. 2005;20:3255–64.
48. Madrakian T, Afkhami A, Zadpour B, Ahmadi M. New synthetic mercaptoethylamino homopolymer-modified maghemite nanoparticles for effective removal of some heavy metal ions from aqueous solution. J. Ind. Eng. Chem. 2015;21:1160–6.
49. Rangabhashiyam S, Anu N, Giri Nandagopal MS, Selvaraju N. Relevance of isotherm models in biosorption of pollutants by agricultural byproducts. J. Environ. Chem. Eng. 2014;2:398–414.
50. Limousin G, Gaudet JP, Charlet L, Szenknect S, Barthès V, Krimissa M. Sorption isotherms: A review on physical bases, modeling and measurement. Appl. Geochemistry. 2007;22:249–75.
51. Kammerer J, Carle R, Kammerer DR. Adsorption and ion exchange: Basic principles and their application in food processing. J. Agric. Food Chem. 2011;59:22–42.
52. Azizian S, Eris S, Wilson LD. Re-evaluation of the century-old Langmuir isotherm for modeling adsorption phenomena in solution. Chem. Phys. 2018;513:99–104.
53. Drago RS, Dias SC, Torrealba M, De Lima L. Calorimetric and spectroscopic investigation of the acidity of HZSM-5. J. Am. Chem. Soc. 1997;119:4444–52.
54. del Piero S, Melchior A, Polese P, Portanova R, Tolazzi M. A Novel Multipurpose Excel Tool for Equilibrium Speciation Based on Newton-Raphson Method and on a Hybrid Genetic Algorithm. Ann. Chim. 2006;96:29–49.
55. Polese P, Tolazzi M, Melchior A. cEST: a flexible tool for calorimetric data analysis. J. Therm. Anal. Calorim. 2018; DOI: 10.1007/s10973-018-7409-2
56. Di Bernardo P, Zanonato PL, Benetollo F, Melchior A, Tolazzi M, Rao L. Energetics and structure of uranium(VI)-acetate complexes in dimethyl sulfoxide. Inorg. Chem. 2012;51:9045–55.
57. Kumar R, Inbaraj BS, Chen BH. Surface modification of superparamagnetic iron nanoparticles with calcium salt of poly(ɣ-glutamic acid) as coating material. Mater. Res. Bull. 2010;45:1603–7.
58. Di Bernardo P, Melchior A, Portanova R, Tolazzi M, Zanonato PL. Complex formation of N-donor ligands with group 11 monovalent ions. Coord. Chem. Rev. 2008;252:1270–85.
59. Del Piero S, Fedele R, Melchior A, Portanova R, Tolazzi M, Zangrando E. Solvation effects on the stability of silver(I) complexes with pyridine-containing ligands studied by thermodynamic and DFT methods. Inorg. Chem. 2007;46:4683–91.

60. Melchior A, Peralta E, Valiente M, Tolazzi M. Solvent effect on heavy metal coordination with thioether ligands: A thermodynamic and theoretical study. Polyhedron. 2014;75:88–94.
61. Jiang W, Lamb JD, Bradshaw JS, Izatt RM, Wu G. High-Specificity Thiacrown Ether Reagents for Silver(I) over Bivalent Mercury and Lead. Thermodynamic and13C NMR Relaxation Time Studies. J. Am. Chem. Soc. 1991;113:6538–41.
62. Hancock RD, Martell AE. Ligand Design for Selective Complexation of Metal Ions in Aqueous Solution. Chem. Rev. 1989;89:1875–914.
63. Yari S, Abbasizadeh S, Mousavi SE, Moghaddam MS, Moghaddam AZ. Adsorption of Pb(II) and Cu(II) ions from aqueous solution by an electrospun CeO2 nanofiber adsorbent functionalized with mercapto groups. Process Saf. Environ. Prot. 2015;94:159–71.
64. Iupac stability constants database. IUPAC & Academic Software; 2005.
65. Giordano TH. Anglesite (PbSO4) solubility in acetate solutions: The determination of stability constants for lead acetate complexes to 85°C. Geochim. Cosmochim. Acta. Pergamon; 1989;53:359–66.
66. Ravichandran M. Interactions between mercury and dissolved organic matter - A review. Chemosphere. Pergamon; 2004. p. 319–31.
67. Fu L, Zhang L, Wang S, Peng J, Zhang G. Silica Nanoparticles Modified with Trithiocyanuric Acid as a Potential Adsorbent for Removal of Ag+ from Aqueous Solutions. Water, Air, Soil Pollut. 2017;228:273.
68. Quang DV, Lee JE, Kim JK, Kim YN, Shao GN, Kim HT. A gentle method to graft thiol-functional groups onto silica gel for adsorption of silver ions and immobilization of silver nanoparticles. Powder Technol. 2013;235:221–7.
69. Xin L, Yin Q, Xin Z, Zhang Z. Powerful adsorption of silver(I) onto thiol-functionalized polysilsesquioxane microspheres. Chem. Eng. Sci. 2010;65:6471–7.
70. Zhang S, Zhang Y, Liu J, Xu Q, Xiao H, Wang X, Xu H, Zhou J. Thiol modified Fe3O4@SiO2 as a robust, high effective, and recycling magnetic sorbent for mercury removal. Chem. Eng. J. 2013;226:30–8.
71. Zhang C, Sui J, Li J, Tang Y, Cai W. Efficient removal of heavy metal ions by thiol-functionalized superparamagnetic carbon nanotubes. Chem. Eng. J. 2012;210:45–52.
72. Zhu H, Shen Y, Wang Q, Chen K, Wang X, Zhang G, Yang J, Guo Y, Bai R. Highly promoted removal of Hg(II) with magnetic CoFe2O4@SiO2 core–shell nanoparticles modified by thiol groups. RSC Adv. 2017;7:39204–15.

73. Odio OF, Lartundo-Rojas L, Palacios EG, Martínez R, Reguera E. Synthesis of a novel poly-thiolated magnetic nano-platform for heavy metal adsorption. Role of thiol and carboxyl functions. Appl. Surf. Sci. 2016;386:160–77.

Figures

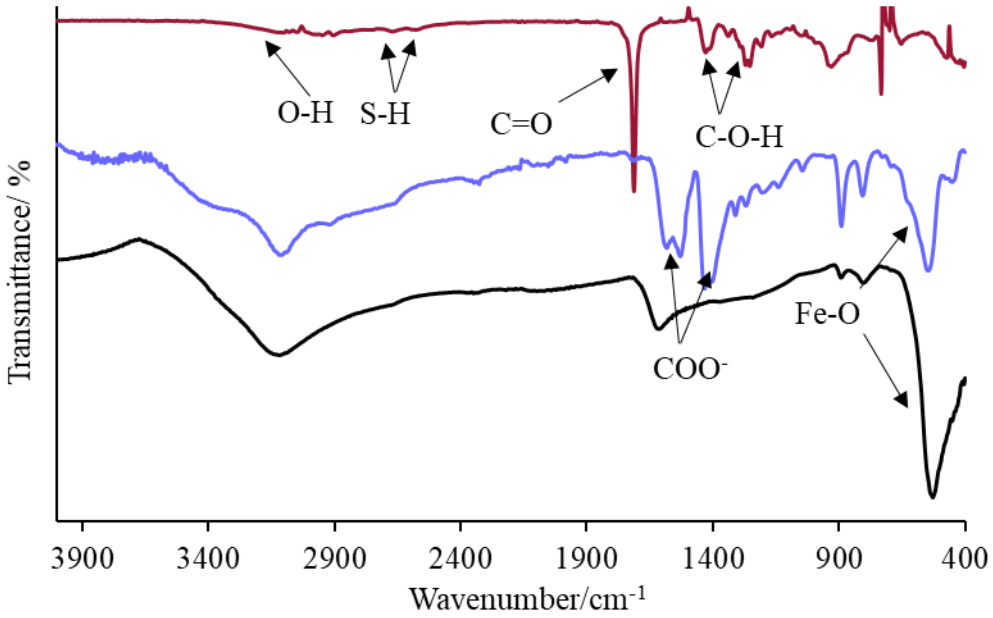

Figure 1. FT-IR spectra of SPION (black), 3-MPA coated SPION (blue) and 3-MPA (red).

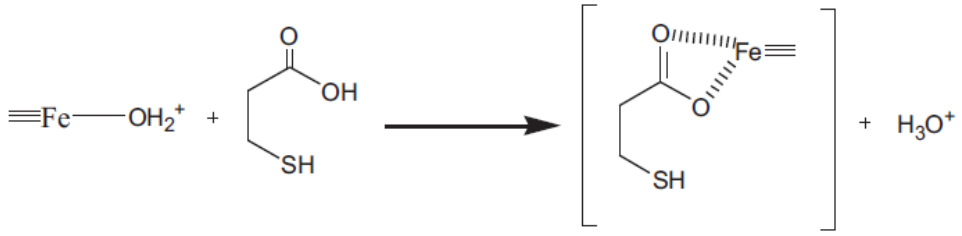

Figure 2. Functionalization mechanism of 3-MPA on SPION (=Fe) surface.

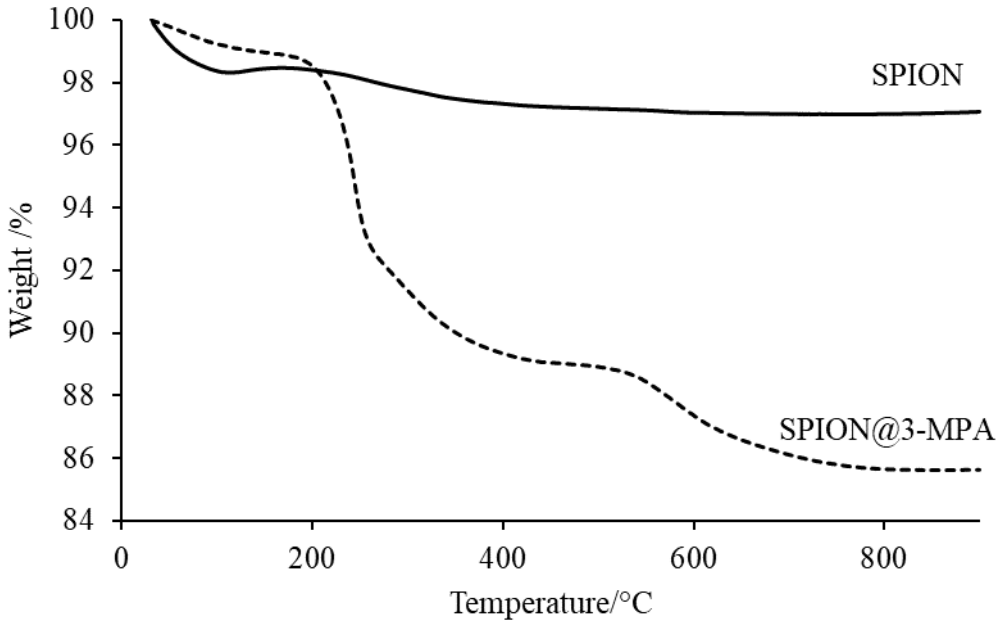

Figure 3. TGA curves for SPION and SPION coated 3-MPA by ligand addition method.

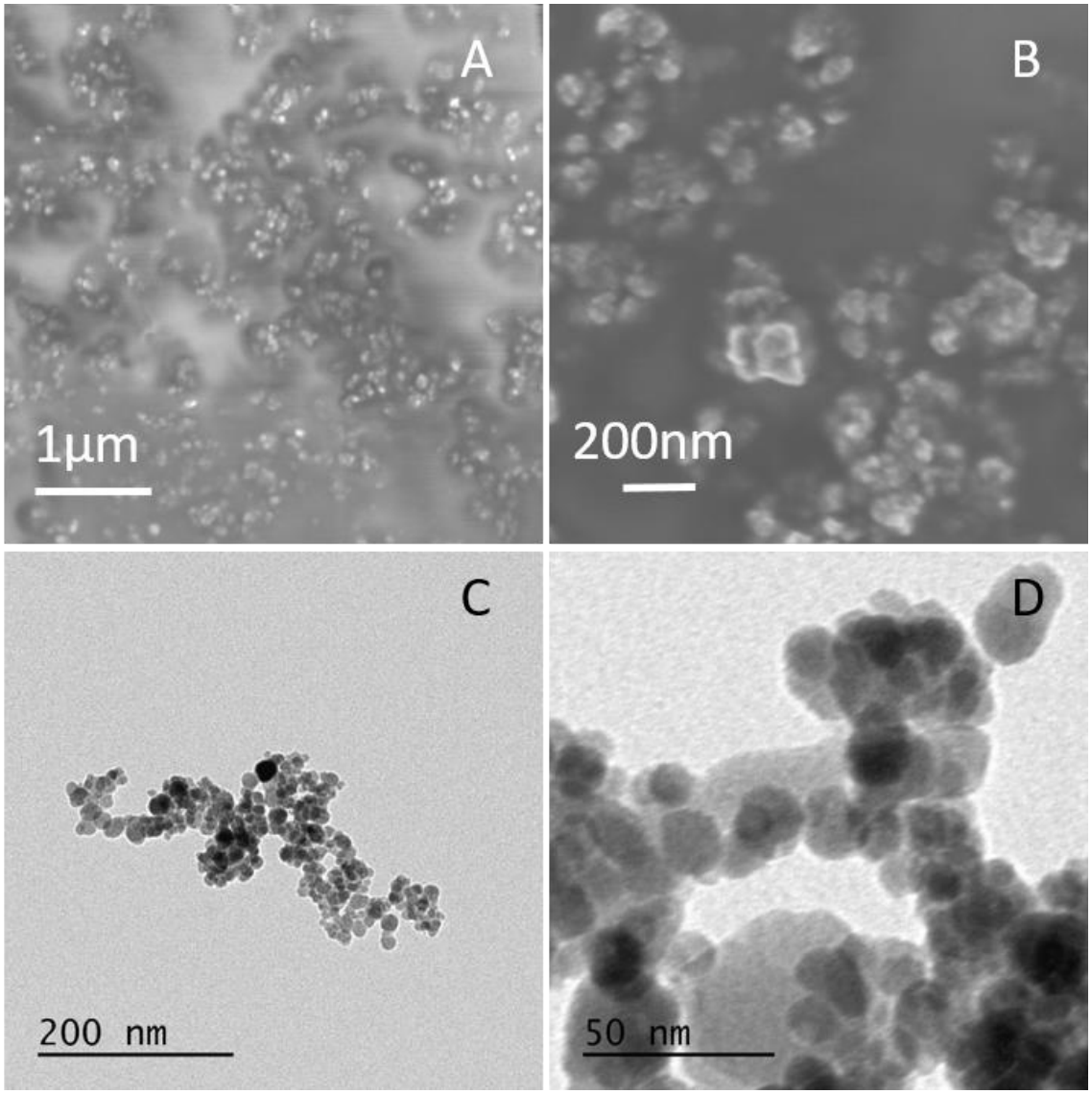

Figure 4. SEM (A,B) and TEM (C,D) images of SPION@3-MPA.

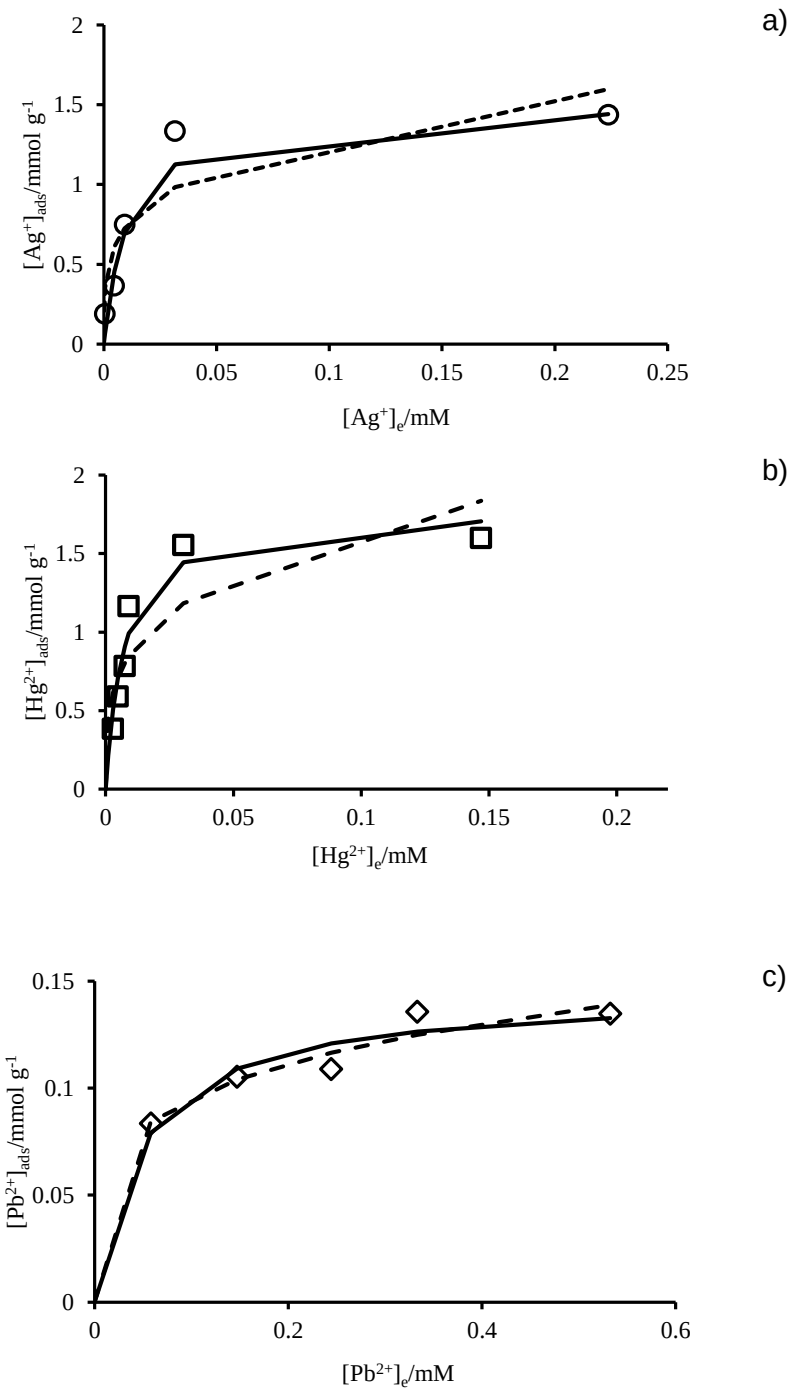

Figure 5. Adsorption isotherms showing the experimental data (symbols) for Ag^{+} (a), Hg^{2+} (b), Pb^{2+} (c) and the calculated values with the best fitting Langmuir (solid line) and Freundlich (dashed line) isotherms (Table 1).

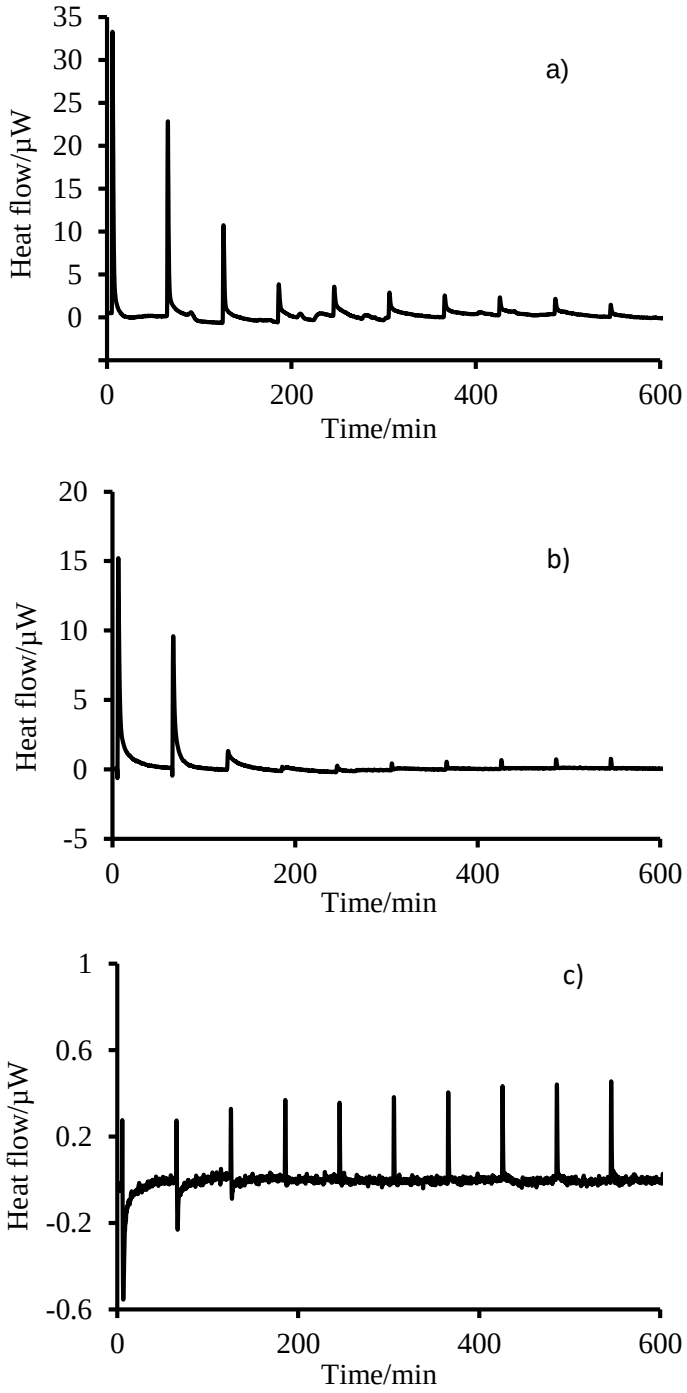

Figure 6. Calorimetric titrations plots corresponding to: 14 injections of 14µL of (a) Ag^{+} 5.0 mM, (b) Hg^{2+} 5.0 mM, (c) 12 injections of 16 µL of Pb^{2+} (4.2mM). The cell contained buffer solution (V = 0.7mL) in which SPION@3-MPA were dispersed (0.5g L^{-1}).

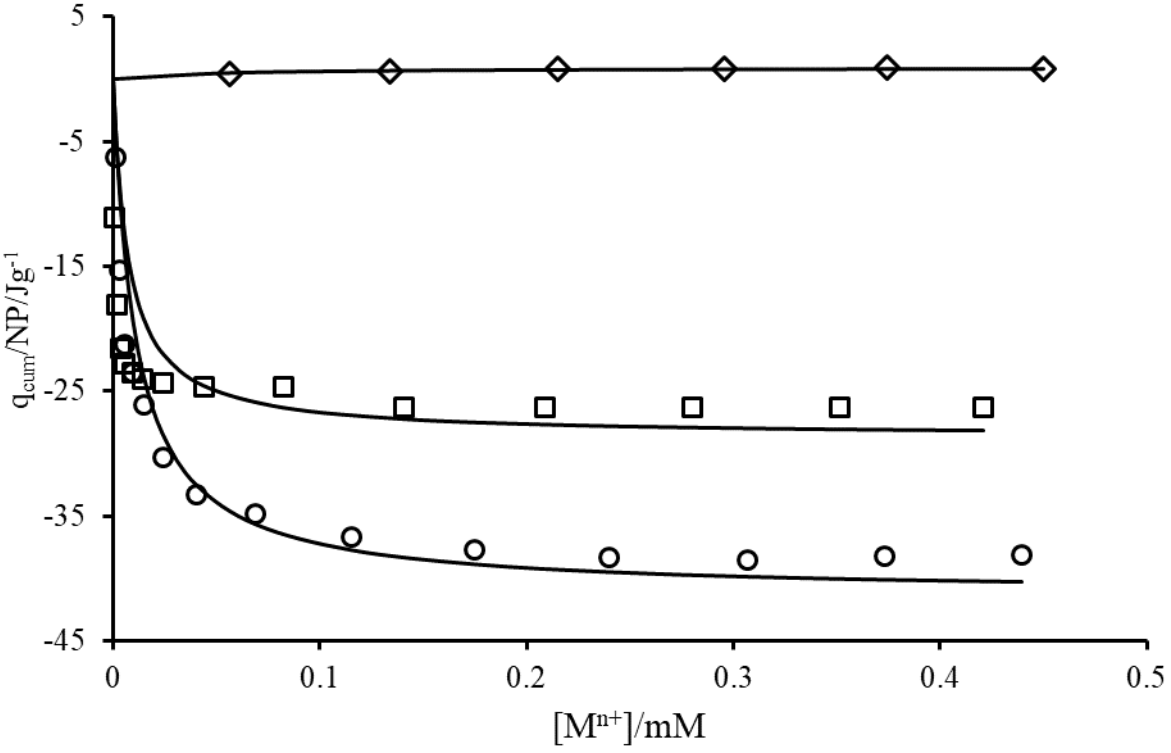

Figure 7. Experimental calorimetric data (points) fitted with eq. 4 (line) for Ag^{+} (○), Hg^{2+} (□) and Pb^{2+} (◇).

Tables

Metal	pH	Langmuir equation				Freundlich equation		
		Q_{max} (mol g^{-1})	b (M^{-1})	log b	R^2	n	K_f (L $mmol^{-1}$ g^{-1})	R^2
Ag^+	5	0.0015 ±0.0001	92482 ±21320	4.9 ±0.2	0.997	4 ±1	2.3 ±0.6	0.879
Hg^{2+}	5	0.0018 ±0.0001	137727 ±32392	5.1 ±0.2	0.998	3.5 ±0.9	3.1 ±0.8	0.837
Pb^{2+}	5	0.00014 ±0.00001	20799 ±7207	4.3 ±0.3	0.986	4.4 ±0.9	0.16 ±0.01	0.943

Table 1. Langmuir and Freundlich isotherms parameters for metal adsorption by SPION@3-MPA.

Metal	ΔG_{ads} (kJ mol^{-1})	ΔH_{ads} (kJ mol^{-1})	ΔS_{ads} (J $mol^{-1}K^{-1}$)
Ag^+	-28.3 ±0.5	-27.2 ±0.7	4 ± 4
Hg^{2+}	-29.3 ±0.5	-17 ±1	41 ± 4
Pb^{2+}	-24.5 ±0.8	6.4 ±0.1	104 ±1

Table 2. Thermodynamic parameters obtained for metal ion adsorption on SPION@3-MPA.

Metal	Adsorbent	S content (mmol g^{-1})	Initial M^{n+} (mM)	Adsorbent dosage (g L^{-1})	pH	Temp. (K)	Contact time (h)	Adsorption capacity (mmol g^{-1})	*b* (M^{-1})	ΔH_{ads} (kJ mol^{-1})	Ref.
Ag^{+}	Silica Nanoparticles Modified with Trithiocyanuric Acid	-	0.46 – 4.63 (50-500mg L^{-1})	2.0	5.0	298	5	0.75 (81.30 mg g^{-1})	806 (7.4711 g L^{-1})	-	[67]
Ag^{+}	Thiol functionalized silica	1.2 (3.79%)	0.9 – 13.3 (96-1436mg L^{-1})	6.7	6.0	298	48	0.703 (75.8 mg g^{-1})	-	-	[68]
Ag^{+}	Thiol-functionalized polysilsesquioxane microspheres	7.60	1 – 150	2	-	273	24	10.57 (1140 mg g^{-1})	-	-	[69]
Ag^{+}	SPION@3-MPA	1.4	0.1 – 1.0	0.5	5.0	298	1[a]	1.5 ±0.1	92481 ±21320	-27.2 ±0.7	This work
Hg^{2+}	$Fe_3O_4@SiO_2$–SH	0.8 (2.64%)	0.02 – 0.50 (5-100mg L^{-1})	0.2	6.5	303	4	0.74 (148.8mg g^{-1})	155 (1.290 g L^{-1})	-	[70]
Hg^{2+}	Thiol-functionalized superparamagnetic carbon nanotubes	6%	0.02 - 0.45 (5-90mg L^{-1})	1	6.5	298	24	0.33 (65.52mg g^{-1})	7883 (0.0393 L mg^{-1})		[71]
Hg^{2+}	$CoFe_2O_4@SiO_2$–SH	-	0.1 – 1.0 (20-200mg L^{-1})	0.05	8	298	12h	3.19 (641.0mg g^{-1})	14241 (0.071 L mg^{-1})	-11.6	[72]
Hg^{2+}	SPION@3-MPA	1.4	0.1 – 1.0	0.5	5.0	298	1[a]	1.7 ±0.1	137727 ±32392	-22.3 ±0.8	This work
Pb^{2+}	Thiol-functionalized superparamagnetic carbon nanotubes	6%	0.02 – 0.43(5-90mg L^{-1})	1	6.5	298	24	0.33 (65.40mg g^{-1})	9375 (0.04525 L mg^{-1})	-	[71]
Pb^{2+}	Poly-thiolated magnetic nano-platform	0.2	0.29 – 1.93 (60-400mg L^{-1})	1.67	-	-	12	0.39 (390µmol g^{-1})	1100 (1.1L $mmol^{-1}$)	-	[73]
Pb^{2+}	ɣ-Fe_2O_3/MPTES	-	0 – 1.16 (0-240mg L^{-1})	6.67	-	298	24	0.46 (96.2mg g^{-1})	-	-	[69]
Pb^{2+}	SPION@3-MPA	1.4	0.1 - 1.0	0.5	5.0	298	1[a]	0.14 ±0.01	20799 ±7168	6.5 ±0.1	This work

Table 3. Parameters of metal adsorption for several thiol-functionalized adsorbents. The original values in the cited references are reported in parentheses. [a]Delay time between metal solution additions.